Int. J. Solids Structures, 1975, Vol. 11, pp. 115–138. Pergamon Press. Printed in Gt. Britain.

FINITE ELEMENT ANALYSIS OF FREQUENCY SPECTRA FOR ELASTIC WAVEGUIDES†

RICHARD J. TALBOT‡ and J. S. PRZEMIENIECKI§
Wright-Patterson Air Force Base, Ohio 45433, U.S.A.

(*Received* 17 *December* 1973; *revised* 25 *March* 1974)

Abstract—The finite element theory is presented for the analysis of the dispersive characteristics of elastic waveguides of arbitrary cross-section. The necessary mass and stiffness properties of circular core, circular sleeve, rectangular, and triangular elements are developed. The practical application of these new elements is demonstrated in the calculation of frequency spectra for circular, square, and triangular waveguides and for a fiber reinforced composite. The dispersive characteristics of the composite material are determined from a formulation which models the fiber as a cylinder and the surrounding matrix material as a rectangular section. The numerical results obtained by the finite element analysis are also compared with the available results from other methods.

1. INTRODUCTION

The dispersive characteristics of bounded elastic media cause a pulse to diminish in amplitude as it propagates due to the different phase velocities of the various components of the pulse. This phenomenon provides an opportunity to develop composite materials which will have desirable pulse attenuation characteristics through selection of density ratios, stiffness ratios, geometric shape and orientation of the various components. Such materials would be of great utility in structures which are subject to high intensity localized transient loads. However, before such designs are possible it is necessary to have an efficient, accurate and simple technique for assessing the influence of the various design parameters on the dispersive characteristics. The analysis developed in this paper provides such a technique for the bounded elastic media (waveguides) of arbitrary cross-section including fiber reinforced composites.

The first theoretical papers devoted to the study of longitudinal wave propagation in an infinitely long isotropic circular cylindrical bar were published by Pochhammer and Chree in 1876 and 1889 respectively[1,2]. These papers contained the first exact formulation of the transcendental equation which relates the admissible frequencies of propagation to the wave number, the so-called frequency equation or dispersion relation. Due to the complicated mathematical nature of the Pochhammer-Chree frequency equation, many years passed before all of its implications were fully appreciated. It was not until the middle of the Twentieth Century that it was fully realized that the exact frequency equation produces an infinite number of branches, called dispersion curves, for each mode of propagation.

† This paper is based on a dissertation submitted by the first author in partial fulfillment of the requirements for the Doctor of Philosophy degree at the Air Force Institute of Technology, Wright-Patterson Air Force Base, Ohio 45433.

‡ Aerospace Engineer, Air Force Flight Dynamics Laboratory.

§ Dean, School of Engineering, Air Force Institute of Technology.

The term mode, in this useage, refers to the type of wave motion, i.e. longitudinal, flexural or torsional and not to resonant frequencies of finite bodies. In addition, the spectra (set of dispersion curves) for each mode contain an infinite set of real branches corresponding to real wave numbers and an infinite set of complex branches corresponding to imaginary and complex wave numbers.

These results are now understood, in a theoretical sense, although the Pochammer-Chree solution is numerically intractable and much too cumbersome for the solution of practical problems. Thus, since the 1950's, much effort has been devoted to the formulation of approximate solutions with the goal of duplicating the first few branches of the exact frequency equation over a limited range of frequencies and wave numbers and usually for a single mode of propagation. The comprehensive review articles by Miklowitz[3], Abramson *et al.*[4], and Redwood[5] describe the development of the many approximate methods which have been advanced and discuss the problem of propagation in noncircular waveguides.

The only prior work using finite element methods for the derivation of the frequency equation is due to Wade[6]. This approach used a mixed force–displacement method of analysis to formulate and investigate the dispersion characteristics of waveguides with cross-sections which consist of an assemblage of rectangular elements of different areas and material properties. The method of formulation would be very cumbersome if applied to sections which consist of a large number of elements because both tractions and displacements must be considered at all element boundaries, a complex procedure which essentially requires manual assembly of the matrix elements.

In this paper several finite elements of a new type have been formulated which greatly facilitate study of the dispersive characteristics of elastic waveguides of arbitrary cross-section. The practical application of these new elements has been demonstrated in the calculation of frequency spectra for circular, square, and triangular waveguides and for a fiber reinforced composite. The dispersive behavior of the composite material has been determined from a formulation which models the fiber as a cylinder and the surrounding matrix material as a rectangular section. The results for the triangular waveguide presented here have not been previously published. The numerical results obtained by the finite element analysis are also compared with the available results from other methods.

2. GENERAL ANALYSIS

The waveguide is defined to be a cylinder of constant cross-section and infinitely long in the z-direction. The cylindrical surface of the waveguide may be generated by any simple closed curve in the x–y plane and the cross-section may be multiply connected. The elastic properties of the waveguide material will be assumed to be constant in the z direction. For stress waves propagating in the z direction the displacement field may be written in the form

$$u(x, y, z, t) = \bar{u}(x, y)\cos(\kappa z - \omega t) \tag{1a}$$

$$v(x, y, z, t) = \bar{v}(x, y)\cos(\kappa z - \omega t) \tag{1b}$$

$$w(x, y, z, t) = \bar{w}(x, y)\sin(\kappa z - \omega t) \tag{1c}$$

where u, v, and w are the displacements in the x, y and z directions, respectively. The parameter κ is the real wave number and ω is the positive, real circular frequency of the propagating stress wave.

It is now advantageous to eliminate the dependence on time by introducing a moving coordinate system x', y' and z' such that

$$x' = x \tag{2a}$$

$$y' = y \tag{2b}$$

$$z' = z - \omega t/\kappa \tag{2c}$$

Hence

$$u = \bar{u} \cos \kappa z' \tag{3a}$$

$$v = \bar{v} \cos \kappa z' \tag{3b}$$

$$w = \bar{w} \sin \kappa z'. \tag{3c}$$

Using these moving coordinates, a single finite element can be isolated from the waveguide, as illustrated in Fig. 1. As in any conventional finite element analysis, approximate displacement functions for $\bar{u}$, $\bar{v}$, and $\bar{w}$ can be selected with some free parameters whose magnitudes can be determined in terms of the designated node displacements, usually on the external boundary of the element, such as u_1 and u_2 at $z' = 0$ and u_3 at $z' = \pi/2\kappa$. In accordance with equations (3) these displacements are the only nonzero displacements at

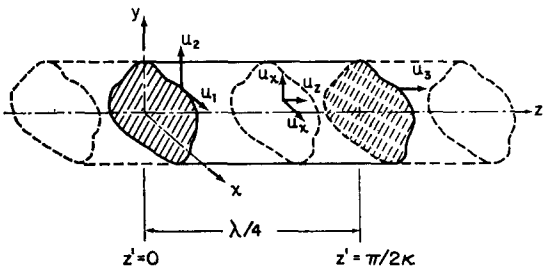

Fig. 1. Waveguide finite element

the cross-sectional planes bounding the finite element. Consequently, it is possible to relate the displacements at any point within the element to the node displacements by means of the matrix equation

$$\begin{bmatrix} u \\ v \\ w \end{bmatrix} = \mathbf{a}(x', y', z') \begin{bmatrix} \mathbf{u}_x \\ \mathbf{u}_y \\ \mathbf{u}_z \end{bmatrix} = \mathbf{au} \tag{4}$$

where $\mathbf{a}$ is a rectangular matrix whose coefficients are functions of x', y', and z', while $\mathbf{u}_x$, $\mathbf{u}_y$, and $\mathbf{u}_z$ are column matrices representing node displacements in the x', y', and z' directions, respectively. The strain distribution within the element, corresponding to the assumed displacement distribution, can now be written in the form

$$\boldsymbol{\varepsilon} = \mathbf{bu} \tag{5}$$

where $\boldsymbol{\varepsilon}$ is a column matrix of all strain components and the matrix $\mathbf{b}$ is obtained by differentiation of the appropriate rows of $\mathbf{a}$ in accordance with the strain–displacement relations of linear elasticity theory.

The equations of motion for a typical element, expressed in terms of the node displacements, can be written as

$$\mathbf{m}\ddot{\mathbf{u}} + \mathbf{k}\mathbf{u} = \mathbf{p} \tag{6}$$

where $\mathbf{m}$ is the mass matrix, $\mathbf{k}$ is the stiffness matrix, and $\mathbf{p}$ represents external loading on the element in the directions of the node displacements[7]. Using equations (1 and 4) it can be shown that

$$\ddot{\mathbf{u}} = -\omega^2\mathbf{u}. \tag{7}$$

Hence, if no external forces are applied, the equations of motion for the element reduce to

$$(-\omega^2\mathbf{m} + \mathbf{k})\mathbf{u} = \mathbf{0} \tag{8}$$

which is of the same form as the standard equation for free oscillations of an elastic system.

It has been demonstrated in [7] that the element mass matrix is calculated from

$$\mathbf{m} = \int_v \rho\mathbf{a}^T\mathbf{a}\,\mathrm{d}V \tag{9}$$

where ρ is the density and the integration is performed over the volume of the element between the two bounding planes $z' = 0$ and $z' = \pi/2\kappa$. Similarly, the element stiffness matrix is calculated from

$$\mathbf{k} = \int_v \mathbf{b}^T\mathbf{E}\mathbf{b}\,\mathrm{d}V \tag{10}$$

where $\mathbf{E}$ is a matrix of the elastic constants in the stress–strain equation

$$\boldsymbol{\sigma} = \mathbf{E}\boldsymbol{\varepsilon}. \tag{11}$$

The computation of the matrix product $\rho\mathbf{a}^T\mathbf{a}$ will contain products of $\sin \kappa z'$ and $\cos \kappa z'$ which when integrated over the element volume will result in a constant factor $\pi/4\kappa$ appearing with the mass matrix $\mathbf{m}$. The computation of the matrix $\mathbf{b}$ will lead to the introduction of the wave number κ as a result of the differentiation. Thus, when the product $\mathbf{b}^T\mathbf{E}\mathbf{b}$ is computed and substituted into equation (10), it is found that the stiffness matrix can be written as the sum of three terms in the form

$$\mathbf{k} = \frac{C}{\kappa}(\mathbf{k}_1 + \kappa\mathbf{k}_2 + \kappa^2\mathbf{k}_3) \tag{12}$$

where C is a constant and $\mathbf{k}_1$, $\mathbf{k}_2$, and $\mathbf{k}_3$ are the three component stiffness matrices. Equation (12) illustrates the explicit dependence of the stiffness matrix on the wave number κ. This dependence is analogous to that which was obtained by Przemieniecki in the formulation of finite element stiffness properties for use in the analysis of local instability of thin-walled structures[8].

Equation (8) for a single element can be assembled into the equations of motion for the complete structure (see Ref [7]), which in this case consist of an assembly of finite elements making up the cross-section and extending over the quarter wavelength ($\lambda/4$) portion of the waveguide. These assembled equations can be denoted symbolically as

$$(-\omega^2\mathbf{M} + \mathbf{K}_1 + \kappa\mathbf{K}_2 + \kappa^2\mathbf{K}_3)\mathbf{U} = \mathbf{0}. \tag{13}$$

Equation (13) can be treated as a real-valued eigenvalue problem in ω^2 by substituting real values for κ and solving for the frequencies ω. The resulting frequency-wave number

relationship gives the real branches of the frequency spectra (family of dispersion curves) for the waveguide, one branch for each degree of freedom. The corresponding eigenvectors (eigenmodes) describe the displacement distribution in the waveguide for each branch. Differentiation of equation (13) with respect to κ leads to an eigenvalue equation for the product of ω and the group velocity $d\omega/d\kappa$. Thus, the solution of both eigenvalue equations could be used to evaluate the group velocity spectra.

3. FINITE ELEMENT MODELS

To represent various cross-sectional geometries of the waveguide, several finite elements have been developed. For circular cross-sections it is necessary to use two types of elements: the core element and the sleeve element, which can also be used for hollow sections (Fig. 2a). For a more general cross-section either triangular or rectangular elements may be employed (Fig. 2b & c). The mass and stiffness properties, as computed by equations (9 and 10), will be presented for two types of core elements, and for sleeve, triangular, and rectangular elements.

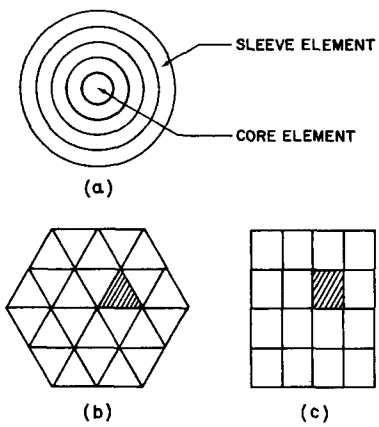

Fig. 2. Cross-sections of waveguide finite slements; (a) circular (axisymmetric), (b) triangular, and (c) rectangular.

Core element

(a) *Linear model.* The simplest model for the assumed displacement distribution (longitudinal wave propagation mode) in the core element is given by

$$\begin{bmatrix} u_z(r, z') \\ u_r(r, z') \end{bmatrix} = \begin{bmatrix} \sin \kappa z' & 0 \\ 0 & \frac{r}{c} \cos \kappa z' \end{bmatrix} \begin{bmatrix} u_1 \\ u_2 \end{bmatrix} = \mathbf{au} \tag{14}$$

where u_1 and u_2 are the node displacements and c is the core radius, as shown in Fig. 3. Due to the symmetry of the motion the node located at $z' = 0$ is actually a "line" node. Thus, the u_2 displacement represents the magnitude of the radial displacement of the outer surface of the bar at $z' = 0$. The u_1 displacement describes the longitudinal motion of the entire bounding plane at $z' = \pi/2\kappa$.

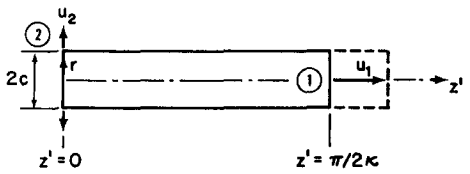

Fig. 3. Linear model for core elements.

Equations (9, 10, 14 and 5) can now be used to determine the mass and stiffness matrices for the linear model of the core element with two degrees of freedom. This leads to the following expression

$$\mathbf{m} = \frac{\pi^2 \rho c^2}{8\kappa} \begin{bmatrix} 2 & 0 \\ 0 & 1 \end{bmatrix} \tag{15}$$

$$\mathbf{k} = \frac{\pi^2 G}{8\kappa} \left(\begin{bmatrix} 0 & 0 \\ 0 & 8(R+1) \end{bmatrix} + \kappa c \begin{bmatrix} 0 & 4R \\ 4R & 0 \end{bmatrix} + \kappa^2 c^2 \begin{bmatrix} 2(R+2) & 0 \\ 0 & 1 \end{bmatrix} \right) \tag{16}$$

where $$R = \frac{2\nu}{1-2\nu} \tag{17}$$

G represents the shear modulus and ν is the Poisson's ratio. It should be noted that the wave number dependence in equation (16) has been expressed in the form previously indicated by equation (12).

(b) *Quadratic model.* If an additional longitudinal displacement node is introduced at the periphery of the element, as shown in Fig. 4, the longitudinal displacement field will then be quadratic in r. The resultant displacement distribution for this case is given by

$$\begin{bmatrix} u_z \\ u_r \end{bmatrix} = \begin{bmatrix} (1-\eta^2)\sin \kappa z' & \eta^2 \sin \kappa z' & 0 \\ 0 & 0 & \eta \cos \kappa z' \end{bmatrix} \begin{bmatrix} u_1 \\ u_2 \\ u_3 \end{bmatrix} \tag{18}$$

where $\eta = r/c$ (19)

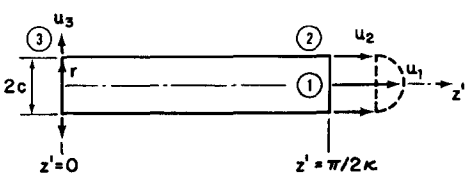

Fig. 4. Quadratic model for core elements.

The resulting mass and stiffness matrices for this three degree of freedom model are

$$\mathbf{m} = \frac{\pi^2 \rho c^2}{24\kappa} \begin{bmatrix} 2 & 1 & 0 \\ 1 & 2 & 0 \\ 0 & 0 & 3 \end{bmatrix} \tag{20}$$

and

$$\mathbf{k} = \frac{\pi^2 G}{24\kappa} \left(\begin{bmatrix} 12 & -12 & 0 \\ -12 & 12 & 0 \\ 0 & 0 & 24(R+1) \end{bmatrix} + \kappa c \begin{bmatrix} 0 & 0 & 6(R+1) \\ 0 & 0 & 6(R-1) \\ 6(R+1) & 6(R-1) & 0 \end{bmatrix} + \kappa^2 c^2 \begin{bmatrix} 2(R+2) & R+2 & 0 \\ R+2 & 2(R+2) & 0 \\ 0 & 0 & 3 \end{bmatrix} \right). \tag{21}$$

(c) *Higher order models.* The number of terms retained in the polynomial representations of the variations of u_z and u_r with r may be increased through the introduction of displacement derivatives at the nodes. A five degree of freedom model was developed, but it appears that for practical applications it is preferable to use the simpler core models in conjunction with one or more sleeve elements in order to better describe the radial dependence of the displacement distribution.

Sleeve element

The longitudinal cross-section of a typical sleeve element is illustrated in Fig. 5. The element uses four node displacements $u_1 \ldots u_4$ and the radial variation of displacements is assumed to be linear. Hence

$$\begin{bmatrix} u_z \\ u_r \end{bmatrix} = \begin{bmatrix} [1 + \frac{1}{t}(r_1 - r)]S & \frac{1}{t}(r - r_1)S & 0 & 0 \\ 0 & 0 & [1 + \frac{1}{t}(r_1 - r)]C & \frac{1}{t}(r - r_1)C \end{bmatrix} \begin{bmatrix} u_1 \\ u_2 \\ u_3 \\ u_4 \end{bmatrix} \tag{22}$$

where

$$S = \sin \kappa z' \tag{23}$$

$$C = \cos \kappa z' \tag{24}$$

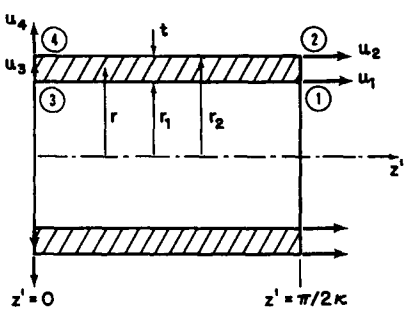

Fig. 5. Sleeve element.

The mass matrix is given by

$$\mathbf{m} = \frac{\pi^2 \rho r_2^2 (d-1)}{24\, d^2 \kappa} \begin{bmatrix} (d+3) & (d+1) & 0 & 0 \\ & (3d+1) & 0 & 0 \\ & & (d+3) & (d+1) \\ & \text{sym} & & (3d+1) \end{bmatrix} \tag{25}$$

where

$$d = r_2/r_1 \tag{26}$$

and the stiffness matrix by

$$\mathbf{k} = \frac{\pi^2 G}{24\kappa} \frac{d-1}{d^2} \left(\kappa^2 r_2{}^2 \begin{bmatrix} (R+2)(d+3) & (R+2)(d+1) & 0 & 0 \\ & (R+2)(3d+1) & 0 & 0 \\ & & (d+3) & (d+1) \\ \text{sym} & & & (3d+1) \end{bmatrix} \right.$$

$$+ \kappa r_2 \frac{2d}{d-1} \begin{bmatrix} 0 & 0 & R(d-4)+d+2 & (R+1)(2d+1) \\ & 0 & -(R+1)(d+2) & R(4d-1)-(2d-1) \\ & & 0 & 0 \\ & \text{sym} & & 0 \end{bmatrix}$$

$$+ \frac{6d^2(d+1)}{(d-1)^2}$$

$$\left. \times \begin{bmatrix} 1 & -1 & 0 & 0 \\ & 1 & 0 & 0 \\ & & 2(R+2)\dfrac{d^2 1\text{nd}}{d^2-1} - 4(R+1)\dfrac{d-1}{d+1} & -2(R+2)\dfrac{d 1\text{nd}}{d^2-1} \\ & \text{sym} & & 2(R+2)\dfrac{1\text{nd}}{d^2-1} + 4(R+1)\dfrac{d-1}{d+1} \end{bmatrix} \right) \tag{27}$$

Triangular element

The triangular waveguide element is depicted in Fig. 6. The element contains six nodes and its state of deformation is described by a column matrix which consists of nine components, $u_1 \ldots u_9$. The first three components describe the longitudinal displacements while the fourth through ninth specify the transverse displacements.

The displacements u, v, and w within the element are assumed to be given by

$$\begin{aligned} u(x', y', z',) &= (c_1 x' + c_2 y' + c_3)\cos \kappa z' \\ v(x', y', z',) &= (c_4 x' + c_5 y' + c_6)\cos \kappa z' \\ w(x', y', z',) &= (c_7 x' + c_8 y' + c_9)\sin \kappa z' \end{aligned} \tag{28}$$

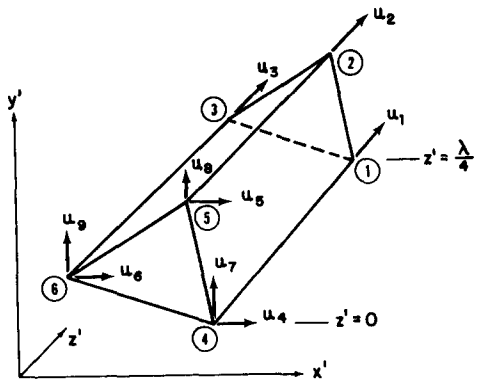

Fig. 6. Triangular element.

where the constants $c_1 \ldots c_9$ can be evaluated in terms of $u_1 \ldots u_9$ in order to obtain the matrix **a** in equation (4). The result is

$$\mathbf{a} = \begin{bmatrix} \mathbf{a}' \cos \kappa z' & \mathbf{0} & \mathbf{0} \\ \mathbf{0} & \mathbf{a}' \cos \kappa z' & \mathbf{0} \\ \mathbf{0} & \mathbf{0} & \mathbf{a}' \sin \kappa z' \end{bmatrix} \tag{29}$$

where

$$\mathbf{a}' = \frac{1}{2A_{123}} [(-y_{32}(x' - x_3') + x_{32}(y' - y_3')) \quad (y_{31}(x' - x_1') - x_{31}(y' - y_1'))$$
$$(-y_{21}(x' - x_2') + x_{21}(y' - y_2'))] \tag{30}$$

$$y_{ij} = y_i' - y_j'; \; i, j = 1, 2, 3 \tag{31}$$

$$x_{ij} = x_i' - x_j'; \; i, j = 1, 2, 3 \tag{32}$$

$$A_{123} = \tfrac{1}{2}(x_{31}y_{32} - x_{32}y_{31}); \text{ area of the triangle } 1, 2, 3. \tag{33}$$

Using equations (9 and 29) it can be easily demonstrated that the mass matrix is given by

$$\mathbf{m} = \frac{\pi \rho A_{123}}{48\kappa} \begin{bmatrix} \mathbf{m}_1 & \mathbf{0} & \mathbf{0} \\ \mathbf{0} & \mathbf{m}_1 & \mathbf{0} \\ \mathbf{0} & \mathbf{0} & \mathbf{m}_1 \end{bmatrix} \tag{34}$$

where

$$\mathbf{m}_1 = \begin{bmatrix} 2 & 1 & 1 \\ 1 & 2 & 1 \\ 1 & 1 & 2 \end{bmatrix}. \tag{35}$$

The corresponding stiffness matrix is of the form

$$\mathbf{k} = \frac{\pi A_{123} G}{48\kappa}\left(\frac{3}{(A_{123})^2}\begin{bmatrix}\mathbf{k}_{11} & \mathbf{0} & \mathbf{0}\\ \mathbf{0} & \mathbf{k}_{12} & \mathbf{k}_{14}\\ \mathbf{0} & \mathbf{k}_{14}^T & \mathbf{k}_{13}\end{bmatrix} + \frac{2\kappa}{A_{123}}\begin{bmatrix}\mathbf{0} & \mathbf{k}_{21} & \mathbf{k}_{22}\\ \mathbf{k}_{21}^T & \mathbf{0} & \mathbf{0}\\ \mathbf{k}_{22}^T & \mathbf{0} & \mathbf{0}\end{bmatrix} + \kappa^2\begin{bmatrix}(R+2)\mathbf{k}_{31} & \mathbf{0} & \mathbf{0}\\ \mathbf{0} & \mathbf{k}_{31} & \mathbf{0}\\ \mathbf{0} & \mathbf{0} & \mathbf{k}_{31}\end{bmatrix}\right) \tag{36}$$

where

$$\mathbf{k}_{11} = \mathbf{k}_{11x} + \mathbf{k}_{11y} \tag{37}$$

$$\mathbf{k}_{11x} = \begin{bmatrix}x_{32}^2 & -x_{32}x_{31} & x_{32}x_{21}\\ & x_{31}^2 & -x_{31}x_{21}\\ \text{sym} & & x_{21}^2\end{bmatrix} \tag{38}$$

$$\mathbf{k}_{11y} = \begin{bmatrix}y_{32}^2 & -y_{32}y_{31} & y_{32}y_{21}\\ & y_{31}^2 & -y_{31}y_{21}\\ \text{sym} & & y_{21}^2\end{bmatrix} \tag{39}$$

$$\mathbf{k}_{12} = (R+2)\mathbf{k}_{11y} + \mathbf{k}_{11x} \tag{40}$$

$$\mathbf{k}_{13} = (R+2)\mathbf{k}_{11x} + \mathbf{k}_{11y} \tag{41}$$

$$\mathbf{k}_{14} = \begin{bmatrix}-(R+1)x_{32}y_{32} & (Rx_{31}y_{32} + x_{32}y_{31}) & -(Rx_{21}y_{32} + x_{32}y_{21})\\ (Rx_{32}y_{31} + x_{31}y_{32}) & -(R+1)x_{31}y_{31} & (Rx_{21}y_{31} + x_{31}y_{21})\\ -(Rx_{32}y_{21} + x_{21}y_{32}) & (Rx_{31}y_{21} + x_{21}y_{31}) & -(R+1)x_{21}y_{21}\end{bmatrix} \tag{42}$$

$$\mathbf{k}_{21} = \begin{bmatrix}-(R-1)y_{32} & (Ry_{31} + {}_3y_2) & (-Ry_{21} + y_{32})\\ -(Ry_{32} + y_{31}) & (R-1)y_{31} & -(Ry_{21} + y_{31})\\ (-Ry_{32} + y_{21}) & (Ry_{31} + y_{21}) & -(R-1)y_{21}\end{bmatrix} \tag{43}$$

$$\mathbf{k}_{22} = \begin{bmatrix}(R-1)x_{32} & -(Rx_{31} + x_{32}) & (Rx_{21} - x_{32})\\ (Rx_{32} + x_{31}) & -(R-1)x_{31} & (Rx_{21} + x_{31})\\ (Rx_{32} - x_{21}) & -(Rx_{31} + x_{21}) & (R-1)x_{21}\end{bmatrix} \tag{44}$$

and the $\mathbf{k}_{31}$ submatrix is equal to the matrix $\mathbf{m}_1$ given by equation (35).

Rectangular element

The rectangular waveguide element is shown in Fig. 7. The model consists of eight nodes and twelve displacement degrees of freedom. For this model the assumed displacement distributions are of the form

$$\begin{aligned} u(x', y', z') &= (A + Bx' + Cy' + Dx'y')\cos \kappa z'\\ v(x', y', z') &= (A' + B'x' + C'y' + D'x'y')\cos \kappa z'\\ w(x', y', z') &= (A'' + B''x' + C''y' + D''x'y')\sin \kappa z' \end{aligned} \tag{45}$$

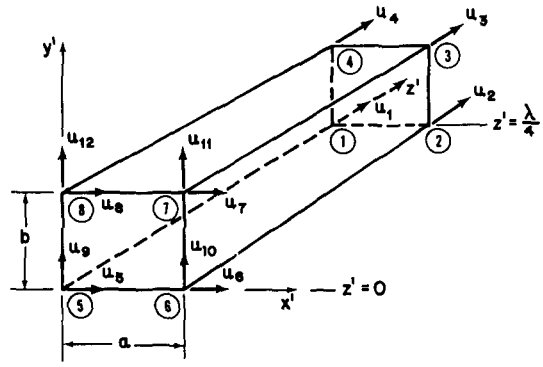

Fig. 7. Rectangular element.

where A, A', A'', $B \ldots$ etc. are constants. The matrix $\mathbf{a}$ is of the same form as for the triangular element, given by equation (29), except that the matrix $\mathbf{a}'$ becomes

$$\mathbf{a}' = [(1 - \xi - \eta + \xi\eta) \quad (\xi - \xi\eta) \quad \xi\eta \quad (\eta - \xi\eta)] \tag{46}$$

where

$$\xi = x'/a \tag{47}$$

$$\eta = y'/b. \tag{48}$$

Using the above matrix $\mathbf{a}'$ in equations (29 and 9) it can be shown that the mass matrix is given by

$$\mathbf{m} = \frac{\pi\rho ab}{144\kappa}\begin{bmatrix} \mathbf{m}_1 & \mathbf{0} & \mathbf{0} \\ \mathbf{0} & \mathbf{m}_1 & \mathbf{0} \\ \mathbf{0} & \mathbf{0} & \mathbf{m}_1 \end{bmatrix} \tag{49}$$

where

$$\mathbf{m}_1 = \begin{bmatrix} 4 & & \text{sym} & \\ 2 & 4 & & \\ 1 & 2 & 4 & \\ 2 & 1 & 2 & 4 \end{bmatrix} \tag{50}$$

The stiffness matrix is given by

$$\mathbf{k} = \frac{\pi abG}{144\kappa}\left(12\begin{bmatrix} \mathbf{k}_{11} & \mathbf{0} & \mathbf{0} \\ \mathbf{0} & \mathbf{k}_{12} & \mathbf{k}_{14} \\ \mathbf{0} & \mathbf{k}_{14}{}^T & \mathbf{k}_{13} \end{bmatrix} + \kappa\begin{bmatrix} \mathbf{0} & \mathbf{k}_{21} & \mathbf{k}_{22} \\ \mathbf{k}_{21}{}^T & \mathbf{0} & \mathbf{0} \\ \mathbf{k}_{22}{}^T & \mathbf{0} & \mathbf{0} \end{bmatrix} + \kappa^2\begin{bmatrix} (R+2)\mathbf{k}_{31} & \mathbf{0} & \mathbf{0} \\ \mathbf{0} & \mathbf{k}_{31} & \mathbf{0} \\ \mathbf{0} & \mathbf{0} & \mathbf{k}_{31} \end{bmatrix}\right) \tag{51}$$

where

$$\mathbf{k}_{11} = \frac{1}{2a^2}\mathbf{k}_{11a} + \frac{1}{2b^2}\mathbf{k}_{11b} \tag{52}$$

$$\mathbf{k}_{11a} = \begin{bmatrix} 2 & -2 & -1 & 1 \\ & 2 & 1 & -1 \\ & & 2 & -2 \\ \text{sym} & & & 2 \end{bmatrix} \tag{53}$$

$$\mathbf{k}_{11b} = \begin{bmatrix} 2 & 1 & -1 & -2 \\ & 2 & -2 & -1 \\ & & 2 & 1 \\ \text{sym} & & & 2 \end{bmatrix} \tag{54}$$

$$\mathbf{k}_{12} = \frac{(R+2)}{2a^2}\mathbf{k}_{11a} + \frac{1}{2b^2}\mathbf{k}_{11b} \tag{55}$$

$$\mathbf{k}_{13} = \frac{1}{2a^2}\mathbf{k}_{11a} + \frac{(R+2)}{2b^2}\mathbf{k}_{11b} \tag{56}$$

$$\mathbf{k}_{14} = \frac{3}{4ab}\begin{bmatrix} R+1 & R-1 & -(R+1) & -(R-1) \\ -(R-1) & -(R+1) & R-1 & R+1 \\ -(R+1) & -(R-1) & R+1 & R-1 \\ R-1 & R+1 & -(R-1) & -(R+1) \end{bmatrix} \tag{57}$$

$$\mathbf{k}_{21} = \frac{3}{a}\begin{bmatrix} -2(R-1) & 2(R+1) & R+1 & -(R-1) \\ -2(R+1) & 2(R-1) & R-1 & -(R+1) \\ -(R+1) & R-1 & 2(R-1) & -2(R+1) \\ -(R-1) & R+1 & 2(R+1) & -2(R-1) \end{bmatrix} \tag{58}$$

$$\mathbf{k}_{22} = \frac{3}{b}\begin{bmatrix} -2(R-1) & -(R-1) & R+1 & 2(R+1) \\ -(R-1) & -2(R-1) & 2(R+1) & R+1 \\ -(R+1) & -2(R+1) & 2(R-1) & R-1 \\ -2(R+1) & -(R+1) & R-1 & 2(R-1) \end{bmatrix} \tag{59}$$

and the submatrix $\mathbf{k}_{31}$ is equal to the matrix $\mathbf{m}_1$ given by equation (50).

4. NUMERICAL EXAMPLES

To illustrate the broad applicability of the finite element determination of waveguide frequency spectra, several types of waveguides were investigated. A circular waveguide was used to establish the manner in which the finite element frequency spectrum converges to the known exact solution due to Pochhammer-Chree. A rectangular waveguide was then analyzed and the results compared to those of prior approximate techniques. Since the finite element method developed in this study is not limited by the geometrical form of the waveguide cross section, the frequency spectra for a triangular cross section, previously unavailable, were also determined. As a final example of the scope of the technique, a fiber reinforced composite was investigated and the results compared with experimental and theoretical results.

Only the real valued portions of the spectra have been computed and presented because the results were obtained through use of a standard, real valued eigenvalue/eigenvector

subroutine (NROOT). A polynomial solving procedure could be used, at least in cases with a limited number of degrees of freedom to produce the complex portions of the branches. All programs were written in extended Fortran and run on a CDC 6600 computer.

Circular waveguide

The physical parameters used in the analysis were the same as those used by Zemanek[9] who has performed an extensive numerical investigation of the exact solution due to Pochhammer-Chree for an aluminium circular waveguide. Consideration was restricted to longitudinal mode propagation, since the circular waveguide element properties previously derived are only appropriate for this mode (axi-symmetrical mode).

The cross section of the rod was subdivided into several equal thickness coaxial elements as indicated in Fig. 2(a) and the radius of the core element was set equal to the thickness of the sleeve elements. If the core element is not included, the model would represent longitudinal mode propagation in a hollow cylinder or shell. Furthermore, if the elements are subdivided into groups with different physical properties, the model would be appropriate for the study of composite circular bars or shells.

The criteria for nontrivial solutions for the nodal displacements given by equation (13) is that the determinant of the coefficients be equal to zero. The results of this condition and the exact solution are shown for the first branch of the frequency spectrum in Fig. 8. For

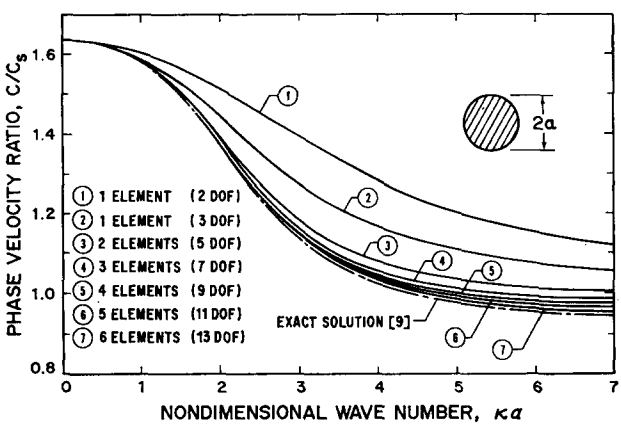

Fig. 8. First branch of the frequency spectrum for the longitudinal mode of propagation in a circular waveguide (Poisson's ratio $\nu = 0{\cdot}3317$).

this comparison, the phase velocity $C = \omega/\kappa$ has been plotted against wave number, the former having been nondimensionalized by division by the shear velocity $C_s = \sqrt{G/\rho}$ and the latter by multiplication by the bar radius a. It can be seen that the method converges to the exact solution as the number of elements and the number of degrees of freedom (DOF) are increased and that only six elements are required to essentially duplicate the exact dispersion characteristics of the first branch throughout the wave number range, with only a slight error (1.5 per cent) in frequency at large values of the wave number.

The finite element frequency equation produces as many branches as there are degrees of freedom in the model. The behavior of the higher order branches is best illustrated by plotting the nondimensional frequency Ω, defined by

$$\Omega^2 = \frac{\omega^2 \rho a^2}{G} \tag{60}$$

as the ordinate. The first four branches, plotted in this manner are shown in Fig. 9.

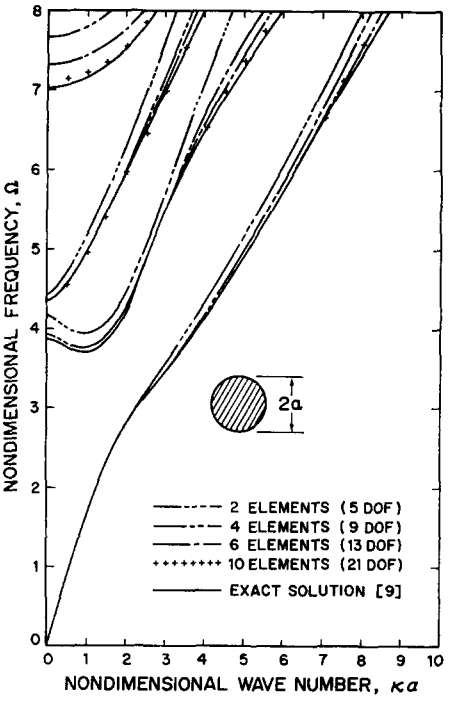

Fig. 9. First four branches of the frequency spectrum for the longitudinal mode of propagation in a circular waveguide (Poisson's ratio $\nu = 0{\cdot}3317$).

The convergence behavior of the finite element idealizations to the exact solution for each branch is evident. As the number of elements is increased, the frequency rapidly converges to the exact value for small wave numbers and the lower branches but converges more slowly as the wave number increases. This is due to the fact that the displacement field becomes more complex as the wave number increases. The displacement distributions given by the finite element solution were compared with the exact solution and it was evident that the large displacement gradients which occur at high wave numbers can be represented accurately with a large number of sleeve elements.

Rectangular waveguide

As a result of the symmetry properties of the rectangular waveguide only one quadrant of the cross section need be considered. The finite elements were defined by subdivision of this quadrant into rectangular subregions of equal dimensions as shown in Fig. 2(c). Both

the longitudinal and torsional modes were investigated. The longitudinal mode was obtained by suppressing the degrees of freedom corresponding to displacements in the plane of the cross section normal to the internal boundaries of the quadrant. The torsional mode was investigated by suppressing the longitudinal displacements along these boundaries. The suppression is performed by setting the appropriate degrees of freedom to zero which is done by elimination of the corresponding rows and columns from the structural matrices. A square bar was assumed in the analysis and a value of one-third was used for Poisson's ratio. The dimensionless frequency given by equation (60) was used as the dependent variable with the characteristic length, a, defined to be the half-width of the bar.

The results for the longitudinal mode will be described first. An investigation of the convergence of the frequency spectra was performed by subdividing the quadrant into 4, 9, 16, 25 and 36 elements. The five lowest frequencies of the 36 element model differed from the corresponding values of the 25 element model by less than one percent for wave numbers less than 3.50. The observed rate of convergence, as expected, was similar to that observed in the case of the circular waveguide and it was apparent that the first several branches had essentially converged in the case of the 36 element model. The frequency spectra for the first ten branches, as generated by this model, are shown in Fig. 10. The branches labeled L are

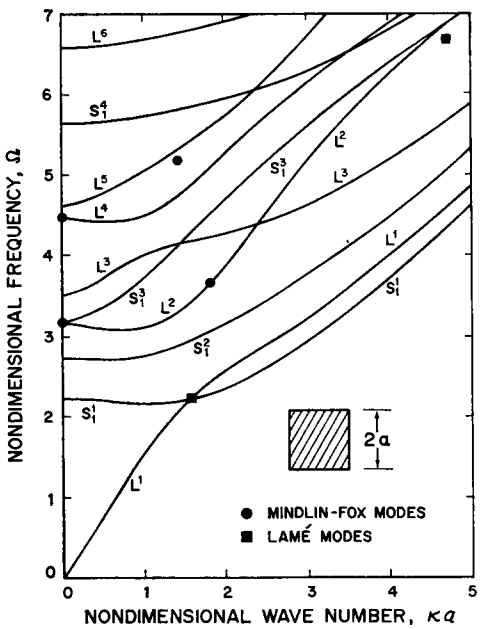

Fig. 10. Longitudinal mode spectrum for a square bar waveguide (Poisson's ratio $\nu = 1/3$, 36 element model).

the longitudinal branches while those labeled S_1 are the so-called screw branches of the square bar. The subscript on the S branches follows the nomenclature used by Fraser[10] to distinguish this type of motion from that which occurs in the torsional mode and which is referred to by Fraser as S_2 motion.

The branch crossings shown in Fig. 10 were determined by investigation of the displacement fields in the vicinity of the crossover points. The crossing of the second and third

longitudinal branches is particularly interesting since it has apparently not been detected previously.

The results shown in Fig. 10 compare very favorably with those published by Fraser[11]. Fraser utilized the displacement fields from the circular rod and the method of collocation to obtain dispersion curves in the rectangular bar. In his first paper on this topic[10] he obtained the first one or two branches for each mode (longitudinal, flexural and torsional) and pointed out that the method would not produce accurate results for the higher branches nor for rectangular bars with width to depth ratios greater than two. There is no reason to believe that the finite element formulation is limited by either of these considerations, although a large number of elements may be required if a very high degree of accuracy is desired. In the case of bars with width to depth ratios greater than two it would probably be desirable to use additional subdivisions of the longer semiaxis when subdividing the cross section into elements. However, this is a procedural detail which adds no additional complication to the analysis.

The first five longitudinal branches shown in Fig. 10 are all but indistinguishable from those presented in Fraser's note[11]. As observed by Fraser, the Mindlin–Fox exact solutions, which include the Lamé modes as a special case, also fall on the predicted spectra, as shown in Fig. 10. The sixth branch lies several percentage points above Fraser's but this is to be expected because the displacement field for such a high order branch would require additional elements for an accurate representation. The very good agreement between Fraser's results and those of the finite element analysis suggests that his collocation method produces a small positive frequency error at large wavelength in a fashion almost identical to that previously described for the finite element analysis. This conclusion is substantiated by the increasing difference between his branches and the experimental data.

The 36 element model was also used to obtain the torsional mode spectra for a square bar. The results, for Poisson's ratio equal to one-third are shown in Fig. 11. Due to the symmetry properties of the square bar, some of these branches are of the screw type. These branches correspond to transverse displacement fields which are symmetric about the diagonals of the bar and are referred to as the S_2 branches by Fraser[10].

Triangular waveguide

The triangular waveguide element shown in Fig. 6 has been used to investigate the dispersive characteristics of an equilateral triangle waveguide with Poisson's ratio equal to one-third. The parameter, a, which is used in the expressions for the dimensionless frequency and wave number was defined to be one-half the side length of the triangle.

Since an analysis of this type of waveguide had not been performed previously, an initial investigation was conducted where in all modes of propagation were retained in the solution. The cross section was subdivided into equilateral subregions to form the finite elements. A typical model consisting of nine elements is illustrated in Fig. 12. Initially, models containing 1, 4, 9, 16 and 36 elements were utilized. This preliminary investigation revealed that several of the branches of the frequency spectra correspond to repeated roots of the frequency equation. The first branch, for example, pertains to flexural motion about both the 1–1 and 2–2 centroidal axes shown in Fig. 12. Furthermore, an examination of the complete set of displacement fields revealed that it was possible to simplify the finite element models by representing only the portion of the waveguide on the right-hand side of a cutting plane which passes through the centroidal axis and the line labeled 1–1 in Fig. 12. This type of idealization will be referred to as a half-bar model. The possible modes of

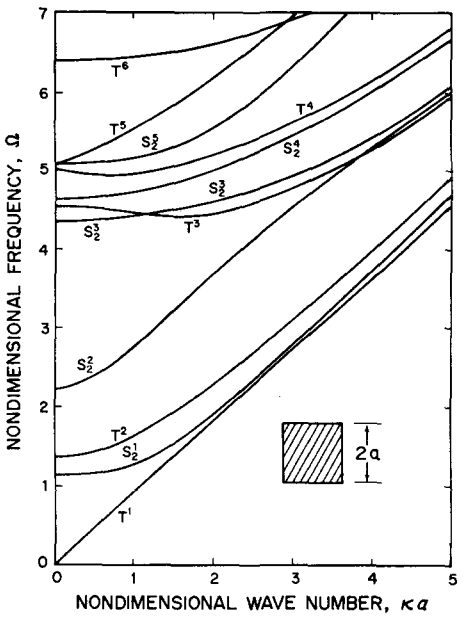

Fig. 11. Torsional mode spectrum for a square bar waveguide (Poisson's ratio $\nu = 1/3$, 36 element model).

motion can then be subdivided into two groups such that each group may be obtained separately by enforcing the proper displacement boundary conditions on the cutting plane.

The first group of modes contains displacement fields which are symmetric with respect to the cutting plane. This group contains the longitudinal mode and the 2–2 axis flexural mode. It also contains a type of mode which is unique to the equilateral triangle waveguide. This mode has been named the symmetric screw mode, *SS*, for reasons which will become apparent subsequently. The second group consists of modes for which the y and z components of the displacement vector are antisymmetric with respect to the cutting plane. These are the torsional mode, flexural mode about the 1–1 axis and another screw type of motion called the antisymmetric screw, or *AS* mode.

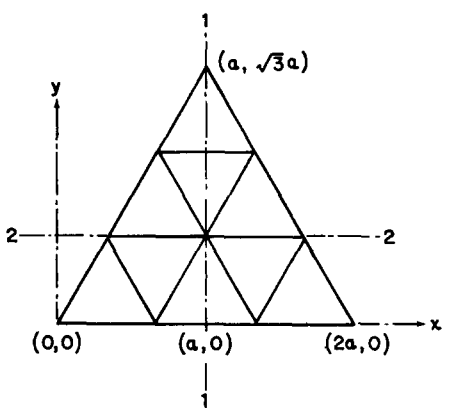

Fig. 12. Nine element idealization of the equilateral triangle waveguide (half-bar 6 element model).

The symmetric modes can be obtained from the half-bar model by setting the x component of the displacement vector to zero at all nodal points which lie on the cutting plane. Similarly, the antisymmetric modes will result from letting the longitudinal and y components be zero at these nodes.

As a result of these considerations, a 45 element half-bar model was used to further refine the spectra. This model was equivalent to an 81 element full-bar model and therefore resulted in a considerable improvement in the accuracy of the spectra branches.

The branches have been numbered without regard to the fact that several of them represent two modes of propagation (eigenmodes). Thus, the first branch is labeled number 1 and the terminology $1a$ and $1b$ is used to refer to the two eigenmodes. The displacement field for each branch is described as longitudinal, screw, flexural, or torsional on the basis of the nature of the displacement vector at the centroid of the cross section. Thus, if only the longitudinal displacement component is nonzero the branch is referred to as longitudinal. If the longitudinal displacement component is zero, but one of the transverse components is nonzero, the motion is of either the flexural or screw type. Finally, if all components of the displacement vector vanish at the centroid, the branch corresponds to torsional motion. The complete frequency spectra for the triangular bar waveguide through the 13th branch, obtained from the 45 element half-bar model, are presented in Fig. 13. The mode of propagation corresponding to each branch is given in Table 1. The subscripts on the flexural modes define the axis about which the flexure occurs (see Fig. 12).

For the equilateral triangle waveguide, the three-fold symmetry about lines joining the vertices and centroid results in two modes which, although similar to the screw modes in the square bar, are not completely equivalent. The transverse displacements of the vertices for these two modes are shown in Fig. 14. The dashed lines illustrate the paths followed by

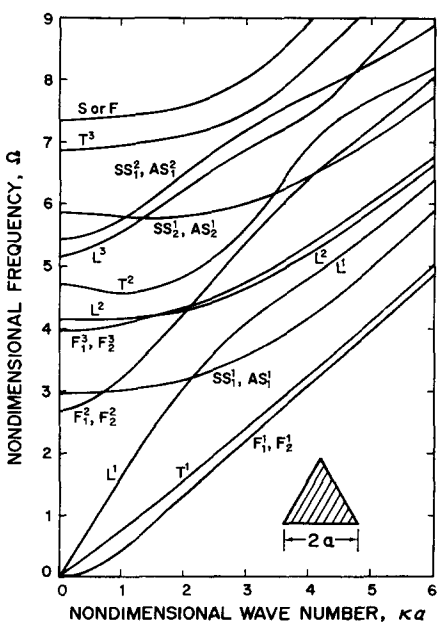

Fig. 13. First thirteen branches of the complete spectra for an equilateral triangle waveguide (Poisson's ratio $\nu = 1/3$, 45 element half-bar model).

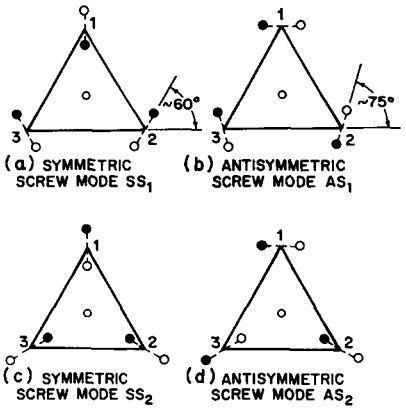

Fig. 14. Symmetric and antisymmetric type 1 and type 2 screw modes for the equilateral triangle waveguide.

Table 1. Modes of propagation corresponding to the first thirteen branches of the frequency spectra for the equilateral triangular bar waveguide

Branch no.	Mode of propagation	Mode terminology
1 *a* & *b*	Flexural	F_1^1, F_2^1
2	Torsional	T^1
3	Longitudinal	L^1
4 *a* & *b*	Flexural	F_1^2, F_2^2
5 *a* & *b*	Screw	SS_1^1, AS_1^1
6 *a* & *b*	Flexural	F_1^3, F_2^3
7	Longitudinal	L^2
8	Torsional	T^2
9	Longitudinal	L^3
10 *a* & *b*	Screw	SS_2^1, AS_2^1
11 *a* & *b*	Screw	SS_1^2, AS_1^2
12	Torsional	T^3
13 *a* & *b*	Screw or flexural	S or F

the vertices during one half-cycle of the motion. The positions of the solid circles indicate the relative locations of the vertices at an extremum of the motion. For convenience of discussion, the uppermost vertex will be referred to as vertex number 1 while the remaining vertices will be referred to as numbers 2 and 3 reading clockwise from number 1.

Figures 14(a) and 14(c) illustrate what have been called the symmetric type 1 and type 2 screw modes. The transverse displacements at the second and third vertices are analogous to the motion at the corners of the square bar for the S_1 and S_2 mode, respectively. However, for the SS_1 mode the motion at vertex number 1 is along the line joining the vertex to the centroid instead of transverse to this line as is the case at the other two vertices. The SS_2 mode is similar to the longitudinal mode except that the motion at vertex number 1 is a half-cycle out of phase with the motion at the other two vertices. This motion may be distinguished from a flexural mode in that the second and third vertices move along the diagonals instead of along paths approximately normal to the line which joins these two vertices.

The AS_2 mode shown in Fig. 14(d) is the antisymmetric counterpart of the SS_2 mode. The antisymmetric type 1 screw mode AS_1, shown in Fig. 14(b), appears to be unique. It

is similar to the F_2 mode if the path of the transverse displacements at the second and third vertices are rotated through approximately 75 degrees to a horizontal plane. This difference appears to be too great to describe this mode as flexural although it appears to be the only feature which distinguishes the two types of motion. The mode shapes for the thirteenth branch are not clearly distinguishable as either a flexural or screw pair.

Several of the mode shapes for the flexural, torsional, longitudinal and screw modes of propagation are shown in Fig. 15. The mode shapes are all given for a constant value of $\kappa a = 0{\cdot}5$. The longitudinal displacement field is shown at the left end of the waveguide element while the transverse displacement field is shown at the opposite end. It should be noted that the scales used to represent the various displacement components are not the same for all modes.

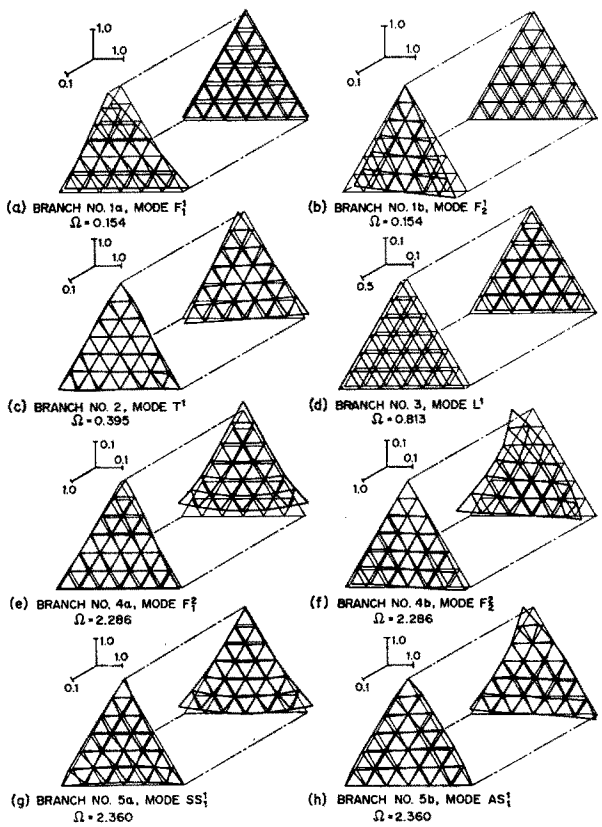

Fig. 15. Typical mode shapes for equilateral triangle waveguides (Poisson's ratio $\nu = 1/3$, Nondimensional wave number $\kappa a = 0{\cdot}5$, 36 element model).

Fiber reinforced composite waveguide

As a final example of the application of the finite element method to the study of elastic wave propagation in waveguides, the dispersive characteristics of a unidirectional fiber reinforced composite were investigated. Both components of the composite were assumed to be homogeneous, linearly elastic, isotropic materials. The direction of propagation was taken to be parallel to the fibers and only the longitudinal mode has been considered.

The composite has been assumed to be infinite in extent in all three coordinate directions. Thus, the dispersive behavior is a direct consequence of the interaction of the stress waves at the interface of the fiber and the surrounding matrix material. Finally, the fibers have been assumed to be equally spaced along each of two orthogonal directions in a plane normal to the fiber axes. A cross section of the composite is shown in Fig. 16. A representative subregion of the cross section, represented by the shaded region, is also shown in the figure.

Since the composite is assumed to be unbounded in the x and y directions the transmission of longitudinal waves in the direction of the fibers will produce no displacements normal to the boundary of the shaded region. The shaded region may therefore be isolated from the remainder of the composite and treated as a waveguide with the stipulation that the appropriate boundary displacements are imposed.

The shaded region in Fig. 16 was assumed to be square, and this permitted the analysis

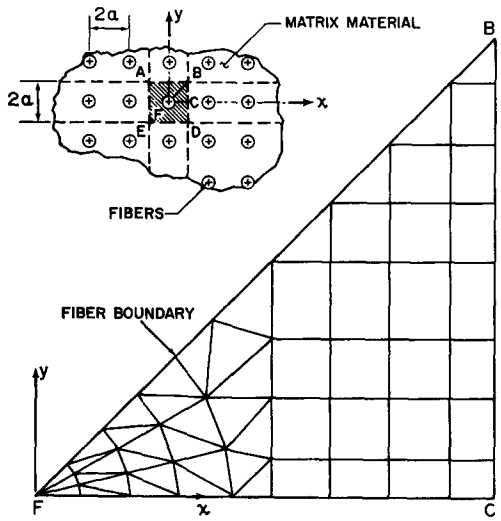

Fig. 16. Finite element model of fiber reinforced composite (55 elements).

to be further restricted to a triangular subregion of the waveguide cross section. This subregion is formed by three planes parallel to the fiber axis which intersect the cross section along the lines labeled BC, FC and FB, where the point F is located at the center of the fiber. The boundary conditions on the plane which passes through BC have been discussed above. Symmetry requires that the y component of displacement must be zero on the plane through FC while x and y displacement components must be of equal magnitude on the plane through FB.

A finite element model of the waveguide is also shown in Fig. 16. The physical and geometric parameters of the model, see Table 2, have been selected to match those of a composite which had been previously investigated both theoretically and experimentally[12].

The parameters, a and C_s, which were used to obtain the dimensionless frequency and wave number were set equal to one-half the distance between the fibers and the velocity of shear waves in the fiber material, respectively. The dispersion relation for the composite,

Table 2. Physical and geometric parameters of the fiber reinforced composite consisting of silica fibers and polystyrene matrix material [12]

Physical parameters	Silica	Polystyrene
Poisson's ratio (ν)	0·17	0·353
Shear modulus, dyne/cm^2, (G)	$3{\cdot}12 \times 10^{11}$	$0{\cdot}1323 \times 10^{11}$
Young's modulus, dyne/cm^2, (E)	$7{\cdot}29 \times 10^{11}$	$0{\cdot}358 \times 10^{11}$
Density, gm/cm^3, (ρ)	2·2	1·056
Geometric Parameters		
Fiber dia, cm,	0·102	
Fiber spacing, cm, ($2a$)	0·236	

depicted in the form of a phase velocity versus wave number relationship, is shown in Fig. 17. The first four branches from the finite element analysis are represented by the continuous curves in the figure.

As mentioned earlier, the composite which was analyzed has been studied previously. Two theoretical formulations referred to as lattice and waveguide models were used in the earlier study. These analyses are much too lengthy to be described here but are discussed in detail in the previously quoted reference. It is of interest to note, however, that the lattice model represented the fiber as having a square cross section while the waveguide model represented the fiber and the surrounding matrix material as concentric circular cylindrical waveguides. Thus, neither model was capable of describing the true geometric configuration of the waveguide. The results of these analyses are also shown in Fig, 17.

Four experimental points on the first branch were also obtained in the earlier study[12]. It will be seen that the finite element first branch phase velocity curve passes very close to these points, with a difference of about 2·5 per cent at $\kappa a = 1{\cdot}17$. The previous analyses had errors of about 4·6 per cent and 8·8 per cent at this value of the dimensionless wave number.

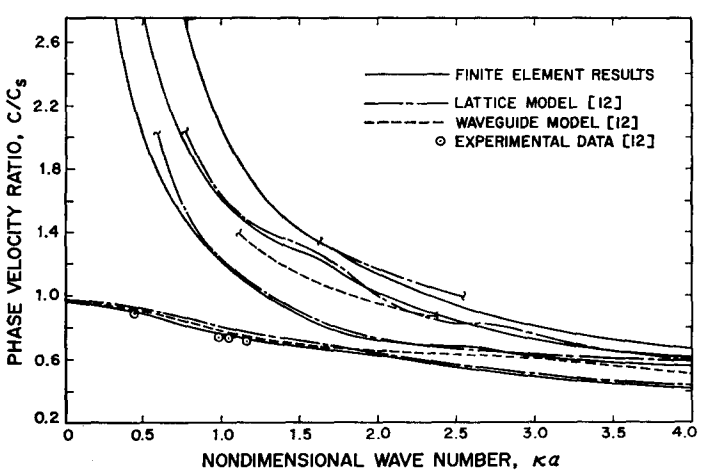

Fig. 17. Frequency spectra for the fiber reinforced composite.

It is interesting to observe that the first branch finite element results correspond to the prior waveguide model results for κa less than 2·0 and then to the lattice model for larger values of κa. For the higher branches, the finite element model agrees very closely with the results of the latice model analysis.

The finite element distribution was determined by considering the nature of the displacement field functions which were anticipated. Thus, it was expected that the dependence of the displacements on the angle between the x axis and the diagonal line, FB, would extend into the region of the fiber. This would almost certainly be true at short wavelength and for the higher branches. The requirement to reflect this type of behavior was met by subdividing the fiber element along radial lines. Furthermore, the fact that the component of displacement normal to each boundary plane must have zero slope in addition to zero magnitude at the boundary suggested that the curvature of these displacement fields would be greater in the vicinity of the boundary. Thus, the matrix material elements adjacent to the boundaries were made somewhat smaller than the interior elements. The finite element model shown in Fig. 16 contains 55 elements (21 fiber and 34 matrix) and it represents 129 degrees of freedom. This model was deemed capable of obtaining at least the first few branches of the longitudinal mode spectra with very good accuracy.

5. CONCLUSIONS

The results of the sample problem investigations clearly illustrate that the finite element method for formulating the frequency equation is simple, efficient, accurate and versatile. In particular, the method can be used to obtain frequency spectra for waveguides of any cross-sectional shape. The necessary mass and stiffness properties for circular core, sleeve. rectangular and triangular elements have been developed and are presented in this paper.

Perhaps one of the most desirable features of the method is its simplicity. The standard form of the frequency equation considerably reduces the complexity of the analysis with respect to other methods. The direct availability of the displacement fields in the form of the eigenvectors facilitates the investigation of branch crossings and determination of displacement behavior for each branch.

REFERENCES

1. L. Pochhammer, Über die Fortpflanzugsgeschwindigkeiten kleiner Schwingungen in einem unbegrenzten isotropen Kreiszylinder *J. reine angew. Math*, **81**, 324–326 (1876).
2. C. Chree, The Equations of an Isotropic Elastic Solid in Polar and Cylindrical Coordinates, their Solutions and Applications, *Transactions of the Cambridge Philosophical Society*, **14**, 250–369 (1889).
3. J. Miklowitz, *Applied Mechanics Surveys*, edited by H. N. Abramson, H. Liebowitz, J. M. Crowley, and S. Juhasz. Spartan Books, Washinton, D. C., pp. 809–839 (1966).
4. H. N. Abramson, H. J. Plass, and E. A. Ripperger, Stress Wave Propagation in Rods and Beams, *Adv. Appl. Mech.* **5**, 111–194 (1958).
5. M. R. Redwood, *Mechanical Waveguides*. Pergamon Press, New York (1960).
6. J. E. Wade, *An Approximate Theory for Elastic Wave Propagation in Multi-bar Media*, Ph.D. Dissertation, Air Force Institute of Technology, Wright-Patterson Air Force Base, Ohio (1970).
7. J. S. Przemieniecki, *Theory of Matrix Structural Analysis*. McGraw-Hill, New York (1968).
8. J. S. Przemieniecki, Finite Element Structural Analysis of Local Instability, *Journal of the American Institute of Aeronautics and Astronautics* **11**, 33–39 (1973).
9. J. Zemanek, An Experimental and Theoretical Investigation of Elastic Wave Propagation in a Cylinder, *Journal of the Acoustical Society of America* **51**, 265–283 (1972).
10. W. B. Frazer, Stress Wave Propagation in Rectangular Bars, *Int. J. Solids Struct.* **5**, 379–397 (1969).
11. W. B. Frazer, Longitudinal Elastic Waves in Square Bars, *J. Appl. Mech.* **37**, 537–538 (1970).
12. W. L. Bade *et al.*, *Shock Wave Dispersion in 3D Reinforced Heat Shield Materials*, Technical Report AFWL-TR-70-91, Vol. I, Air Force Weapons Laboratory (1970).

Абстракт — Дается теория конечного элемента для анализа диссипативных характеристик упругих волноводов произвольного поперечного сечения. Определяются необходимые свойства массы и жесткости для круглой жилы, круглой втулки, прямоугольных и трехугольных элементов. Указывается практическое применение этих новых элементов в расчете спектров частоты для круглых, квадратных и трехугольных волноводов и для усиленных волокнами слоистых материалов. Определяется диссипативная характеристика слоистых материалов на основе формулировки, которая моделирует волокно как цилиндр и материал окружающей среды матрицы в форме прямоугольного сечения. Сравниваются, также, численные результаты, полученные из анализа конечного элемента, с доступными результатами из других методов.